ARCHIVES OF TRANSPORT *ISSN (print):* *0866-9546*
Volume 59, Issue 3, 2021 ***e-ISSN (online):*** *2300-8830*
DOI: *10.5604/01.3001.0015.0093*

THE EFFECT OF DIFFERENT MARSHALLING FORMS ON THE AERODYNAMIC PERFORMANCE OF THE FREIGHT TRAIN UNDER CROSSWIND

Zihao XIE[1], Zhenfeng WU[2], Longhui ZHU[3], Wangcai DING[4]

[1, 2, 3, 4] *School of Mechanical and Electrical Engineering, Lanzhou Jiaotong University, Lanzhou, China*

Abstract:

Different types and quantities of freight cars will affect the marshalling forms of freight trains. In order to investigate the influence of the marshalling forms on the aerodynamic performance of freight trains under crosswind, three types of freight cars such as box cars, gondola cars and tank cars, were selected to marshal with locomotives. This paper used Detached Eddy Simulation method (DES) based on the SST $k-\omega$ turbulent model to simulate the aerodynamic performance of the freight train under crosswind. The wind speed, wind angle and train running speed were set as 25m/s, 45° and 100km/h respectively. The influence of different marshalling forms on the aerodynamic performance of the freight train such as aerodynamic drag and lateral force were calculated and compared. The results showed that the marshalling forms have significant effect on the aerodynamic drag and the maximum difference of the aerodynamic drag can reach 20.5%. Furthermore, the variations of the lateral force of the whole train and the locomotive are not apparent. The maximum difference is only 4.3% and 4.1% respectively. However, the changes of marshalling forms have obvious influence on the lateral force of each carriage. The maximum difference of the lateral force of the box car, gondola car and tank car is 17%, 20.1% and 24.1% respectively. The essential reason why the marshalling forms has a significant impact on the aerodynamic performance of the freight train is that there are obvious differences in the volume and shape structure of each railway carriage. The large volume of box cars and the cavity structure of gondola cars make their position a key factor affecting the aerodynamic performance of freight trains. Among the six different marshalling forms selected in this paper, the best marshalling form is: locomotive--gondola car--box car--tank car. Both the aerodynamic drag of the train and the lateral force of the boxcar are the smallest by taking this marshalling form.

Keywords: *crosswind, freight train, train marshalling, aerodynamic drag, lateral force*

To cite this article:

Xie, Z., Wu, Z., Zhu, L., Ding, W., 2021. The effect of different marshalling forms on the aerodynamic performance of the freight train under crosswind. Archives of Transport, 59(3), 57-71. DOI: https://doi.org/10.5604/01.3001.0015.0093

Contact:
1) 1594751070@qq.com [https://orcid.org/0000-0002-9211-195X] – corresponding author; 2) wzhf@mail.lzjtu.cn [https://orcid.org/0000-0002-8129-4703]; 3) 3172477962@qq.com [https://orcid.org/0000-0001-5734-3520]; 4) XZH1997317@163.com [https://orcid.org/0000-0002-6761-6008]

1. Introduction

In recent years, the stability, safety and aerodynamic performance of High-speed trains under crosswind have become two major concerns. Some scholars focus on studying the impact of the environmental changes on High-speed trains (Baker. 2010; Mao et al., 2011; Xi et al., 2015; Yang et al., 2010). Liu et al. (2020) studied the overturning safety when the train is running under the varying wind speed and suggested the process for estimating a wind speed interval for the safe train operation under the abruptly changing wind speed. Niu et al. (2018) compared the aerodynamic performance of stationary and moving trains with or without windbreak wall under crosswind and found that for a train without a windbreak wall under crosswind, the method for stationary trains can replace that for moving trains to simulate the pressure field around and the aerodynamic forces of a train. There are also some researchers who change the shape of the train to explore the variation in the aerodynamic performance of the train. Wu et al. (2017) investigated a design method for large-scale streamlined head cars of high-speed trains by adopting NURBS theory according to the outer surface characteristics of trains and revealed that the high-speed train with large-scale streamlined head car could achieve the purpose of reducing running aerodynamic drag and saving energy. Huo et al. (2020) researched the impact of the trailing edge shape of a downstream dummy vehicle on train aerodynamics under crosswind and found the obvious differences in the pressure distributions in the streamlined transition areas on the windward sides for the head cars with different end shapes. Chen et al. (2018) analyzed the effect of different nose lengths on train aerodynamic performance under crosswind. The results indicated that the nose length significantly affects the pressure coefficient on the windward side of the head car and the leeward side of the tail car.

Freight trains are one of the important components of the railway transportation system. However, compared with high-speed trains, the aerodynamic performance and operational safety of freight trains under crosswind have not received sufficient attention yet. Although Gao et al. (2004) and Xiong et al. (2015) have researched on the aerodynamic performance of freight cars, the research objects were all single vehicles and the aerodynamic performance of the whole freight trains was not take into consideration. Flynn D et al. (2014,2016) simulated the slipstream of an operational freight train and investigated the effect of crosswinds on the slipstream of a freight train. Sterling et al. (2008) studied the slipstreams of high-speed passenger trains and freight trains. Wu et al. (2018) investigated a design method for streamlined electric locomotives according to the principles of bionics. However, there is only one type of railway vehicle in their research. This article selected three different types of freight vehicles and formed six different marshalling forms. The aerodynamic drag and the lateral force of freight trains in different marshalling forms were calculated and analyzed. The findings could provide references for relevant railway departments to make freight train formation plans.

In this paper, numerical methods and train models were introduced in the upcoming section. The further section describes the numerical simulation, including the validation of the method, computational mesh, computational domain and boundary conditions. Calculation results and associated analysis were presented in the penultimate section. The conclusions were summarized in the final section.

2. Geometrical models and case

There are many kinds of railway freight vehicles. Due to the limitations of the space length and the calculation resources, three typical railway freight vehicles, such as box cars, gondolas and tank cars, are selected to form six different marshalling schemes by changing the positions of each vehicle in the marshalling. The geometrical model was marshalled with four cars, namely, a locomotive, a box car, a gondola car, and a tank car. The difference between the numerical calculation models is that the order of the three freight vehicles is different. The locomotive model and its position and the total length of the train are all fixed. In this paper, the length of the locomotive is 22m, and the lengths of boxcars, gondola cars and tank cars are 16.43m, 13.438m and 11.99m respectively. The total length of the train is 63.389m. The handles, pantographs and other surface protrusions are removed to ensure the accuracy of the calculation results and a certain number of grids. The bogies are also simplified. The dimensions of each vehicle and six different types of calculation models are shown in Figure 1 and Figure 2.

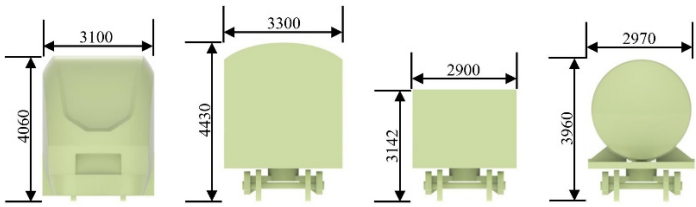

Fig. 1. The dimensions of different railway freight vehicles (unit: mm)

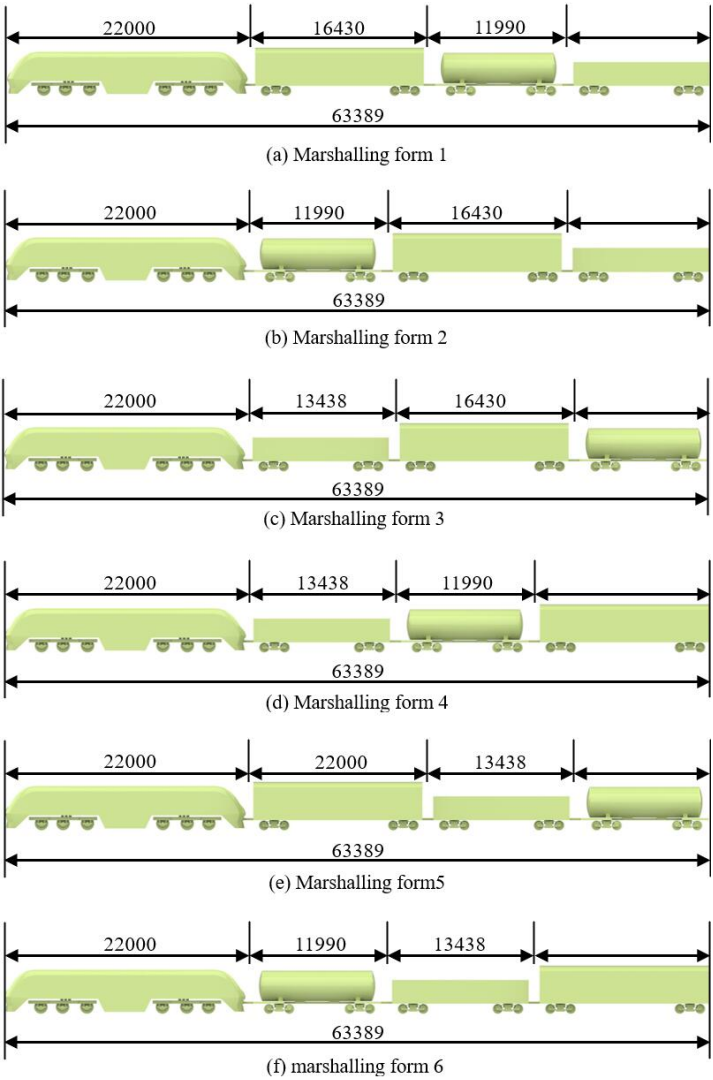

Fig. 2. Train models of different marshalling forms (unit: mm)

The wind angle and the running direction of the train are shown in Figure 3. V_M, V, β are the train speed, the crosswind speed and the wind angle respectively. V_x, V_y are the components of the cross wind in x and y directions respectively. Considering the traction power of the existing locomotive and the future development space, the train speed V_M is set to 100km/h. In this paper, β =45°, V=25m/s, $V_x = V_y$ =17.7 m/s[1].

$$V_x = V \times cos\,\beta \qquad V_y = V \times \sin\beta \tag{1}$$

3. Numerical simulation

3.1. Numerical methods

Large eddy simulation (LES) is an effective method for simulating the flow field. Some researchers simulated the flow around the train in different environments by this method successfully (Östh et al., 2014; Krajnović et al., 2012; Hemida et al., 2010). However, the requirements of this method for the grid on the near wall of the train are extremely strict and the method is computationally quite expensive. The Reynolds averaged Navier–Stokes (RNS) method has lower computational cost and reasonable accuracy in calculating the aerodynamic drag (Cheli et al., 2010). Sima et al. (2015) simulated the flow filed of the train under crosswind and compared the calculation results with the experimental results. The obtained results show that a well-performed RANS CFD can predict the aerodynamic coefficient of streamlined trains with relatively high accuracy. Wang et al. (2018) also obtained effective results when studying the aerodynamic performance of the train under crosswind by the RNS method.

The flow field structure of freight train is more complex because of the large space between the carriages. In order to obtain more accurate simulation results of the flow field and analyze the reasons for the change of the aerodynamic performance of the train, the RNS method was first used to solve the steady flow field in the calculation, and the result obtained was used as the initial condition of the unsteady flow field. Detached eddy simulation (DES) combines the two advantages of LES in capturing vortices with high accuracy and the economy of the Reynolds averaged Navier–Stokes (RNS) method, and it has been widely used in recent years to simulate the flow field of the train under crosswind.

This study used the commercial CFD software Fluent19.0 to simulate the flow filed around the train. The compressibility of air was ignored in the calculation because of the relatively low speed of freight trains. RNS and DES based on the SST $k-\omega$ turbulent model was used to study the aerodynamic performance of the train. SIMPLE (Semi-Implicit Method for Pressure-Linked Equations) algorithm was employed to solve the pressure and velocity coupling equations (Niu et al., 2017). The time integration was conducted using a implicit second-order accurate scheme, and the time step was set as $\Delta t = 5\times10^{-4}$ s, and 35 iterations are performed in each time step.

3.2. Verification of the calculation methods

Zhou et al. (2007) used a combination of wind tunnel test and numerical simulation and got the aerodynamic performance of P64 boxcar and C64 gondola car when running on the embankment. In this paper, the same calculation conditions, train running speed, cross wind speed, calculation domain size and other conditions are set. The surface mesh of the verification model is shown in Figure 4 (a) and (b). The lift and lateral force of the train at different wind speeds are calculated by the DES method.

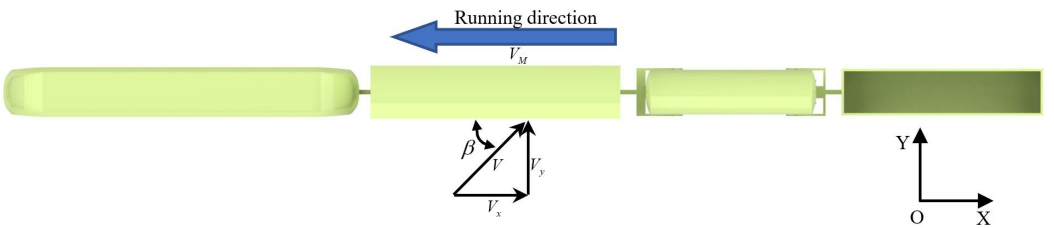

Fig. 3. Schematic of the freight train running under crosswind

Figure 5 shows the comparison between the calculation results in this paper and the literature data. It can be seen from Figure 5 that the simulation results in this paper and the literature data are consistent in the trend, but there are certain errors in specific values. The main reason for the errors is that although the same type of train model is used, the simplification degree of the two is different. Since the maximum error is less than 8.5%, it is considered that the numerical method adopted in this paper can effectively simulate the aerodynamic performance of freight trains under crosswind.

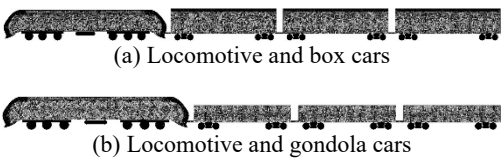

(a) Locomotive and box cars

(b) Locomotive and gondola cars

Fig. 4. Surface mesh of the verification model

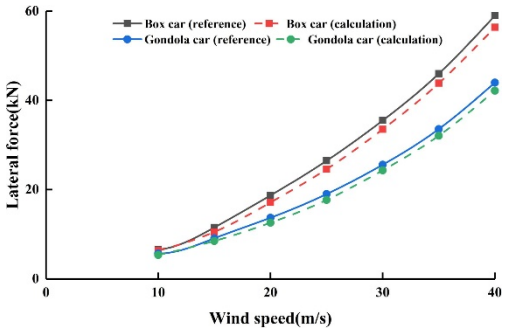

(a) Lateral force

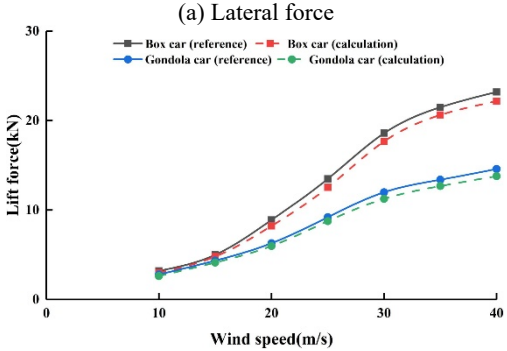

(b)Lift force

Fig. 5. Comparison of numerical simulation results and literature data

3.3. Grid generation

In this paper, ICEM software was used to mesh the computational domain. In order to ensure the calculation accuracy and save the computing resources, structured grids are used in the far-field area, and unstructured grids are used in the near-wall area. Because the head of the locomotive and the tank have a streamlined structure, the grids were encrypted here. In addition, the bogies of each vehicle, the underframe of the tank car and the connecting devices between the vehicles have many parts and small structures. Although the geometric model has been simplified, the meshes of these parts still need to be encrypted. To ensure that the velocity gradients near the wall are correct, 10 layers of boundary layer grids were set on the surface of the car body. The height of the first prism layer is 0.04mm and the growth rate is 1.25. The y^+ value is distributed between 5-75. Figure 6(a) shows the longitudinal center section grid of the computational domain and boundary layer grid. The surface mesh of the locomotive and each car are shown in Figure 6(b).

3.4. Verification of grid independence

In order to ensure the accuracy of the calculation results and eliminate the influence of the number of grids on the simulation, three sets of grids with different densities were selected for calculation, and the variations of the lateral force and the aerodynamic drag of the locomotive with different grid numbers were compared. The results of grid independence verification are shown in Table 1. It can be seen from Table 1 that the calculation error of the three different grids is within 1.5%, and the influence of the number of grids on the accuracy of the calculation results can be ignored. In order to improve the computational efficiency, the first set of grids with about 25 million was selected for numerical calculation.

Table 1. The influence of the number of grids on the calculation results

	Number of grid (million)	Aerodynamic drag of locomotive(N)	Aerodynamic drag of box car(N)	Lateral force of locomotive(N)	Lateral force of box car(N)
Mesh1	25	11517	14724	36108	22677
Mesh2	28	11512	14716	36102	22669
Mesh3	32	11506	14712	36094	22672

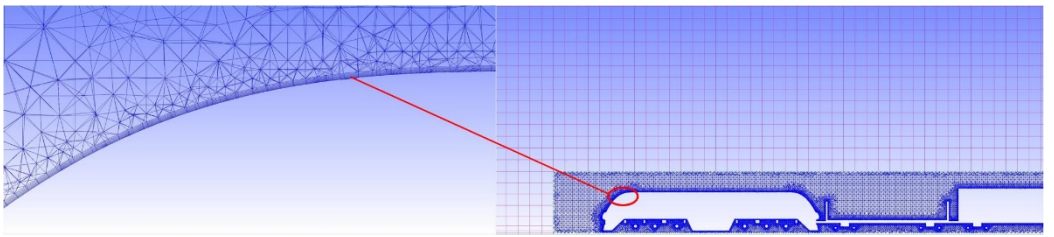

(a) The mesh of the longitudinal center section and boundary layers

(b) Surface mesh of the freight train.

Fig. 6. Computational mesh

3.5. Calculation domain and boundary conditions

The calculation domain is shown in Figure 7. Since the height of each freight train is inconsistent, the total length of the train is selected as the unit length in this paper. The distance from the front of the train to the surface ABCD is L, and the distance from the rear of the train to the surface EFGH is 2L. The height of calculation domain is L. The distance from the windward side of the train to the surface DCEF is L, and the distance from the leeward side of the train to the surface ABGH is 2L. In order to simulate the flow field of the train under crosswind, the surface ABCD is set as the velocity inlet boundary condition, and the incoming flow velocity V_1 is the sum of the train running speed and the wind speed component in the X direction[2]. The surface CDEF is also set as the velocity inlet boundary condition. The incoming flow velocity V_2 is consistent with the component magnitude of the wind velocity in the Y direction[3]. The bottom of the calculation domain (surface BCFH) is set as no-slip moving wall boundary condition, and the moving speed is the same as the train running speed, but the direction is opposite. The top of the computational domain (surface ADEG) is set as the symmetry boundary condition. Both the surface ABGH and the surface EFGH are set as the pressure outlet boundary conditions.

$$V_1 = V_m + V_x \tag{2}$$

$$V_2 = V_y \tag{3}$$

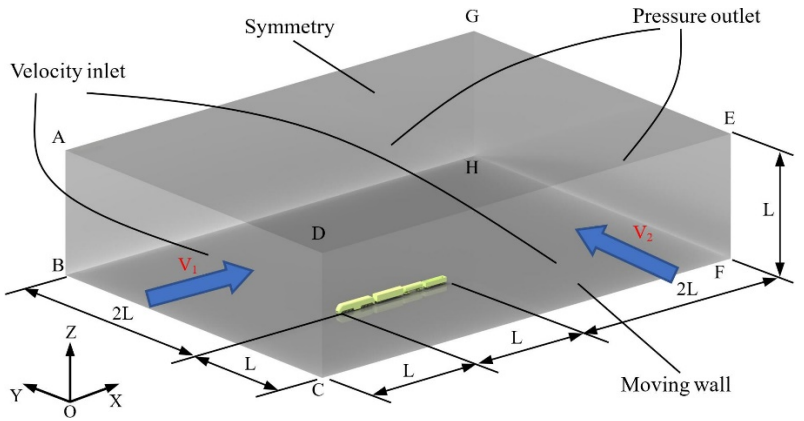

Fig. 7. Calculation domain and boundary conditions

4. Results and discussion

4.1. Analysis of the aerodynamic drag

The aerodynamic drag of each vehicle and the total aerodynamic drag of the train are shown in Figure 8. It can be seen from Figure 8 that when the trains are marshalled according to scheme 3 and scheme 5, the aerodynamic drag is the smallest, which is reduced by 20.5% and 18.1% respectively compared with the maximum value. From the perspective of the marshalling scheme, the common point of these two marshalling forms is that the boxcar and the gondola car are adjacent to each other, and both are in the middle of the whole train. From the data point of view, marshalling form 3 significantly reduces the aerodynamic drag of the boxcar, which is 28.9% lower than the average aerodynamic drag of the boxcar. Marshalling form 5 greatly reduces the aerodynamic drag of the gondola car, which is 34.3% lower than the average value. This form also significantly reduces the aerodynamic drag of the locomotive, which is 14% lower than the average aerodynamic drag of the locomotive. In order to explore the reasons for the influence of the marshalling form on the aerodynamic drag of the train, it is necessary to analyze the variations of the aerodynamic drag of different vehicles under different marshalling forms.

It can be seen from Figure 8 that when marshalling forms 1 and 5 are used, the aerodynamic drag of the locomotive is the lowest, which is reduced by 15.3% and 13.9% respectively compared with the average value of the aerodynamic drag of the locomotive. The common point of these two marshalling forms is that the boxcar is adjacent to the locomotive. Figure 9(a) and 9(e) show that when trains are marshalled according to scheme 1 and scheme 5, the pressure of the area between the driver's cab at the rear of the locomotive and the head of the boxcar (area A and area B) have increased significantly compared to the other four conditions. Since the height and cross-sectional area of boxcars are larger than that of the locomotive, the air flowing through the cab at the rear of the locomotive will inevitably be hindered by the end wall of the box car. This obstruction will increase the surface pressure at the rear of the locomotive, which will reduce the pressure difference between the front and rear of the locomotive. It can be seen from Table 2 that when the trains are marshalled according to scheme 1 and scheme 5, the differential pressure drag of the locomotive decreases by 16.2% and 14.9% respectively compared with the average value. This is the main reason for the reduced aerodynamic drag of the locomotive.

Figure 8 shows that when trains are marshalled according to scheme 3 and scheme 6, the aerodynamic drag of the box car is the lowest, which is reduced by 28.9% and 9.7% respectively compared with the average value of the aerodynamic drag of the box car. The common point of the two types of marshalling forms is that the box car is located at the adjacent rear end of the gondola car. It can be seen from Figures 9(c) and 9(f) that when the boxcar is behind the gondola car, the high-pressure area of the front end wall of the boxcar is significantly reduced compared to other situations. As shown in Figure 9(c) and Figure 9(f), when the air flows through the gondola, it is divided into three parts. The first part of the air flow will flow directly from the top of the gondola car because the height of the gondola is the lowest. When the gondola car is not loaded with cargo, the front end wall, the caudal end wall and the underframe are combined into a semi-closed cavity structure. Since the front end wall and the caudal end wall have a strong obstructive effect on the airflow, most of the airflow forms two vortices of different sizes in the cavity under this obstruction. A small part of the airflow between the two vortexes flows out of the gondola car along the underframe and caudal end wall. Part of the airflow out of the gondola car flows backwards along the top of the boxcar, and the other part forms two vortices of different sizes between the caudal end wall of the gondola car and the front end wall of the box car because of the obstruction of the front end wall of the box car. However, the speed of this part of the airflow is greatly reduced under the hindrance of the caudal end wall of the gondola car, so the impact on the front end wall of the box car is not strong. This is the main reason for the reduced drag of the box car.

When the marshalling form of scheme 6 is adopted, the reduction in aerodynamic drag of the box car is lower than that of scheme 3. That is because the box car is located at the end of the train, and there is a large negative pressure area at the rear of the train. It can be seen from Table 2 that when scheme 6 is adopted, the differential pressure drag of the box car is larger than that of scheme 3. Therefore, in the marshalling form of scheme 6, the reduction in aerodynamic drag of the box car is smaller than that of scheme 3.

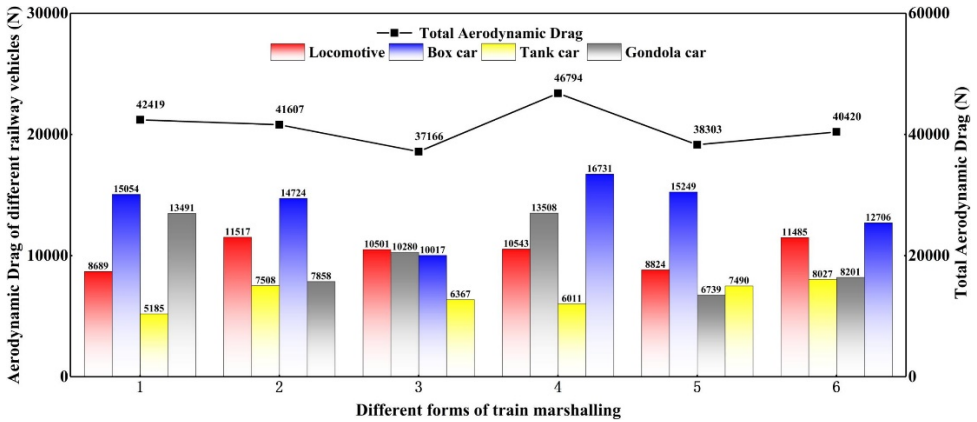

Fig. 8. Aerodynamic drag of different vehicles and total aerodynamic drag of the train

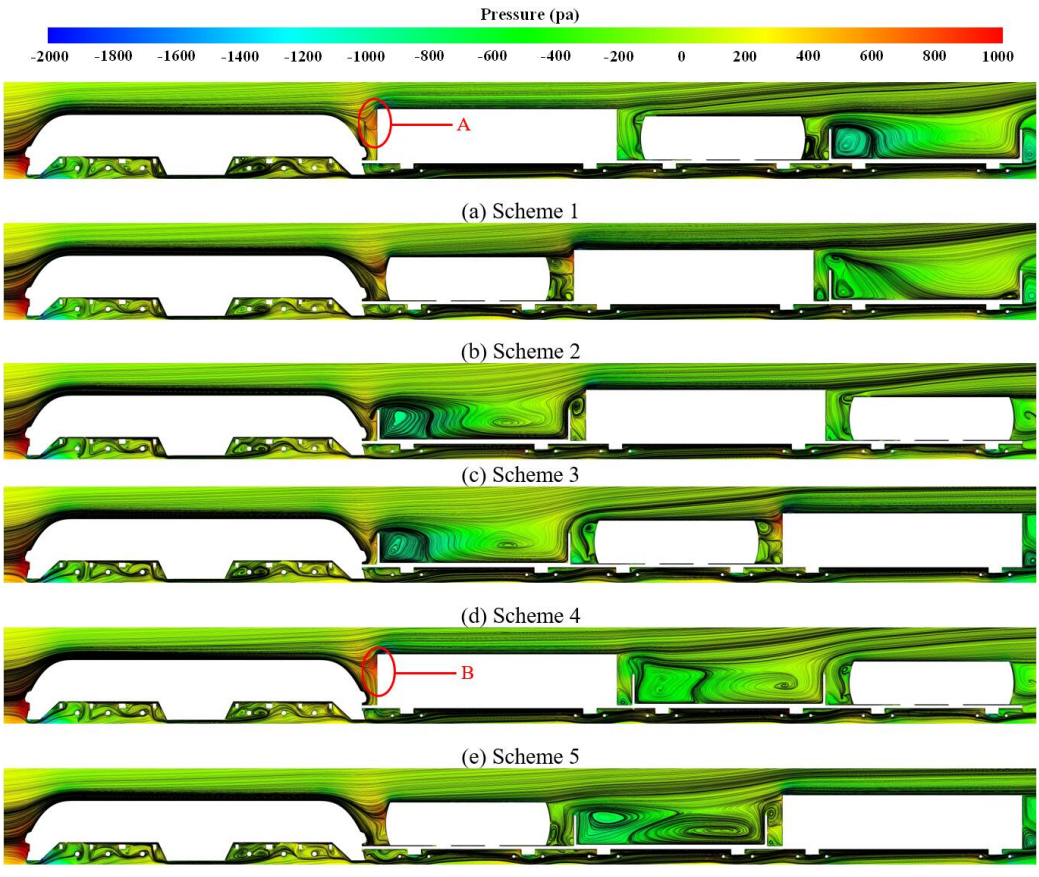

(a) Scheme 1

(b) Scheme 2

(c) Scheme 3

(d) Scheme 4

(e) Scheme 5

(f) Scheme 6

Fig. 9. Streamline and pressure distribution in longitudinal section of trains with different marshalling forms

Table 2. Aerodynamic drag of the different vehicles

Train marshalling	Train type	Differential pressure drag[N]	Frictional drag[N]	Total aerodynamic drag[N]
1	Locomotive	8028.43	660.44	8688.87
	Box car	14593.25	460.81	15054.06
	Tank car	4967.30	218.12	5185.42
	Gondola car	13184.53	306.49	13491.02
2	Locomotive	10842.32	674.71	11517.03
	Tank car	7263.17	245.27	7508.44
	Box car	14277.03	446.71	14723.74
	Gondola car	7596.64	261.22	7587.86
3	Locomotive	9819.55	680.31	10499.86
	Gondola car	9983.57	296.94	10280.51
	Box car	9555.94	461.11	10017.05
	Tank car	6144.01	222.10	6366.11
4	Locomotive	9857.43	685.97	10543.40
	Gondola car	13185.82	321.72	13507.54
	Tank car	5575.82	235.33	5811.15
	Box car	16265.50	465.96	16731.46
5	Locomotive	8160.86	663.47	8824.33
	Box car	14796.78	452.20	15248.98
	Gondola car	6458.22	281.23	6739.45
	Tank car	7243.36	246.61	7489.97
6	Locomotive	10821.40	663.81	11485.21
	Tank car	7788.81	238.20	8027.01
	Gondola car	7973.47	227.79	8201.26
	Box car	12251.71	454.76	12706.47

Due to its small volume and better streamline structure compared with the box car and the gondola car, the aerodynamic drag of the tank car is low. The change of the marshalling form will have varying degrees of influence on the aerodynamic drag of the tank car. However, the aerodynamic drag of the tank car accounts for a relatively small proportion of the total aerodynamic drag of the train, and the impact on the drag of the whole train is limited. Therefore, this paper will analyze no more.

From the above, it can be seen that due to its special semi-open cavity structure, the airflow through the no-load gondola car has aggregation effect, and part of the airflow after the gondola car continues to flow backward, so the aerodynamic drag of the vehicle behind the gondola car will be significantly reduced. Since the height and cross-sectional area of the box car are the largest in the entire train, its obstructive effect on the airflow is very obvious. Figure 10 (a), (b), (c) and (e) show that the area of the high-pressure region on the surface of the vehicle behind the box car is significantly reduced compared to other situations. This obstruction will also act on the vehicle in front of the box car, reducing the differential pressure drag of the preceding car, thereby reducing the aerodynamic drag of the front car. When the trains are marshalled according to scheme 3 and scheme 5, the box car and the gondola car are located in the middle of the train, and both can affect the front and rear cars, thereby greatly reducing the aerodynamic drag of the train.

4.2. Analysis of the lateral force

When the gondola car or box car is at the end of the whole train, the drag reduction effects of both cannot be played at the same time, especially when the box car is at the end and the gondola car is not adjacent to the boxcar (Scheme 4). Since there are no other vehicles behind the box car, it cannot be used to reduce the aerodynamic drag of the rear vehicle. Moreover, due to the large volume of the boxcar, its aerodynamic drag is also very large. When the drag reduction effect of the gondola car does not directly affect the box car, the box car's ability to reduce the drag of the vehicle in front of it cannot offset the large drag effect brought by its own volume. That is the reason why the aerodynamic drag is the largest when the train is marshalled according to scheme 4.

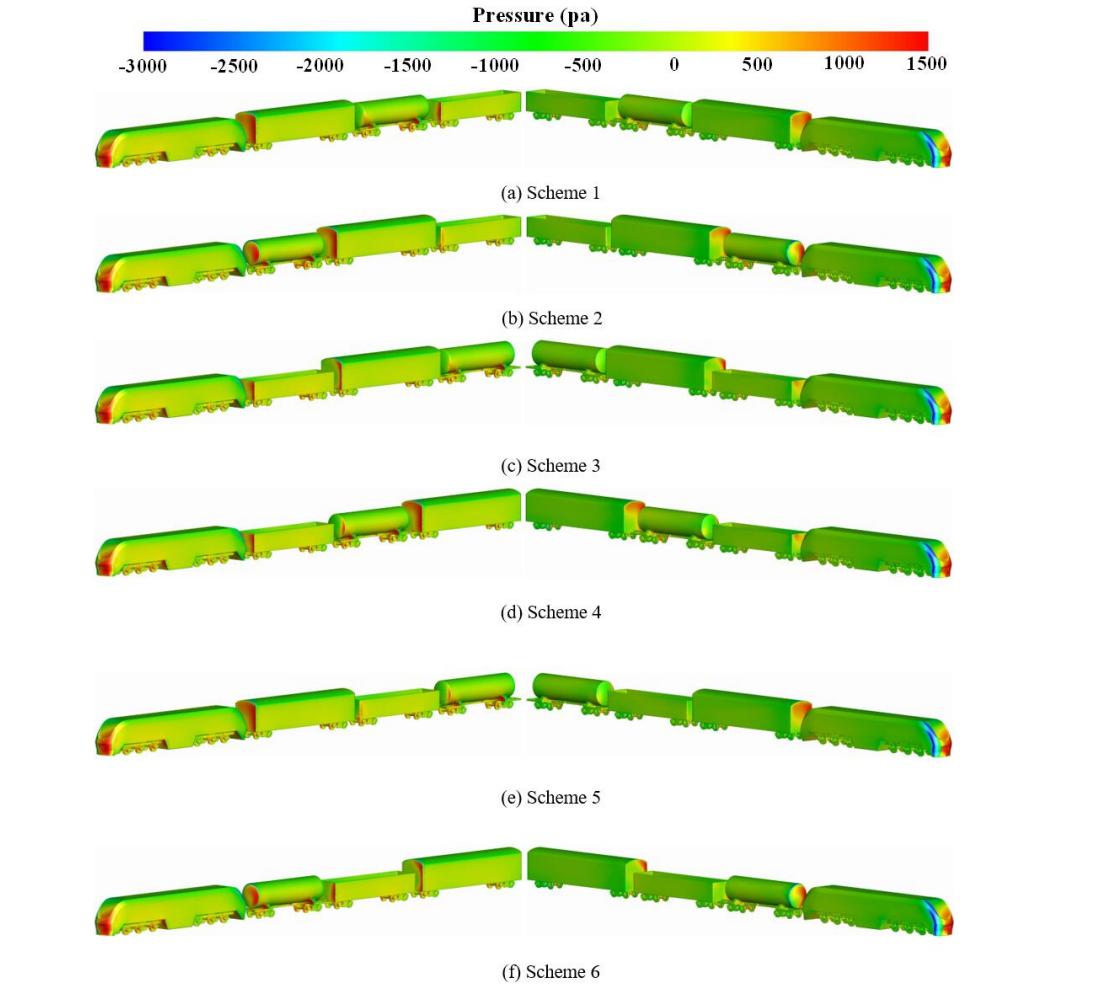

Fig. 10. Pressure distribution of freight trains with different marshalling forms

The lateral force of each freight vehicle is shown in Figure 11. Due to the long length of the locomotive and the large longitudinal section area, the lateral force of the locomotive under crosswind is the maximum. The longitudinal section area of the boxcar is only second to the locomotive's, so the lateral force of the boxcar is only second to the locomotive's. Likewise, the lateral force of the tank car is the smallest, and the lateral force of the gondola car is between that of the box car and the tank car. But the marshalling form has little effect on the total lateral force of the whole freight train. The maximum difference is only 4.3%. For each vehicle, the maximum difference of lateral force of locomotive is 4.1%, and that of box car, gondola car and tank car is 17%, 20.1% and 24.1%, respectively.

Because the height of each freight vehicle is different, and the area of the horizontal section of the tank car varies with the height of the section, the flow field is divided horizontally based on the center height of tank car to research the pressure distribution and streamline in the flow field. The distribution of pressure and streamline at the cut surface are shown in Figure 11.

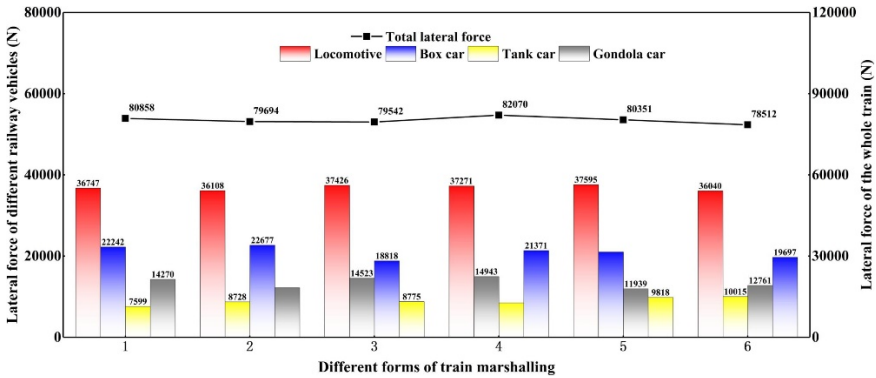

Fig. 11. Lateral force of different vehicles and total lateral force of the train

It can be seen from Figure 11 that when scheme 1 is adopted, the lateral force of the tank car is the minimum, and that of the gondola car is the minimum when scheme 5 is adopted. The common point of these two marshalling forms is that the position of the gondola car and the tank car is the same, that is, the second car behind the locomotive, and both are at the adjacent tail of the box car.

Fig. 12. Schematic diagram of the train horizontal section position

Figure 13 (a) and Figure 13 (e) show that due to the large volume of box car, a considerable part of the airflow is blocked by the box car when gondola car and tank car are behind. Therefore, there is no obvious high pressure area on the windward side of the tank car and the gondola car. The pressure difference between the windward side and leeward side of the vehicle is reduced, which results in the decrease of the lateral force of the vehicle.

It can be seen from Figure 13 (a)-(f) that when the crosswind flows through the locomotive, part of it continues to flow backward along the side wall of the locomotive on the windward side, while the other part continues to flow backward along the front cab of the locomotive to the leeward side of the train. Since freight trains do not have a windshield structure, and the distance between each car is long, part of the airflow will pass through the gap between the cars and flow along the front end wall of the rear car perpendicular to the direction of train. The air flow passing through the gap between carriages and the airflow that continues to flow backward on the leeward side of the train passing through the cab at the locomotive head merge with each other to form a vortex. Because the box car has a large cross-sectional area and a strong blocking effect on the airflow, more airflow flows through the front end wall of the boxcar, and the collision with the airflow flowing backward from the leeward side is intenser. That is why the vortex volume formed near the front end wall of the leeward side of the boxcar is the largest.

Figure 13 (b) and 13 (d) show that when the boxcar is at the rear of the tank car, the vortex on the leeward side of the boxcar is significantly larger than that in other cases. That is because the front and rear ends of the tank are curved when viewed from the horizontal section, making the distance between the tank car and the box car short in the middle and long on both sides. Part of the air flowing between the box car and the tank car is strongly obstructed by the front end wall of the box car, and then changes the direction of flow and moves closer to the rear of the tank car. That part of the airflow merges with the airflow flowing backward on the leeward side of the train to form the periphery of the vortexes, which is the main reason for the increase in the volume of the vortexes on the leeward side. Another part of the airflow flows along the front end wall of the boxcar to the leeward side. That part of the airflow will form the central part of the vortexes after meeting with the airflow flowing backward on the leeward side. As shown in Figure 13 (b) and 13 (d), due to the increase in the volume of the vortex, the area of the

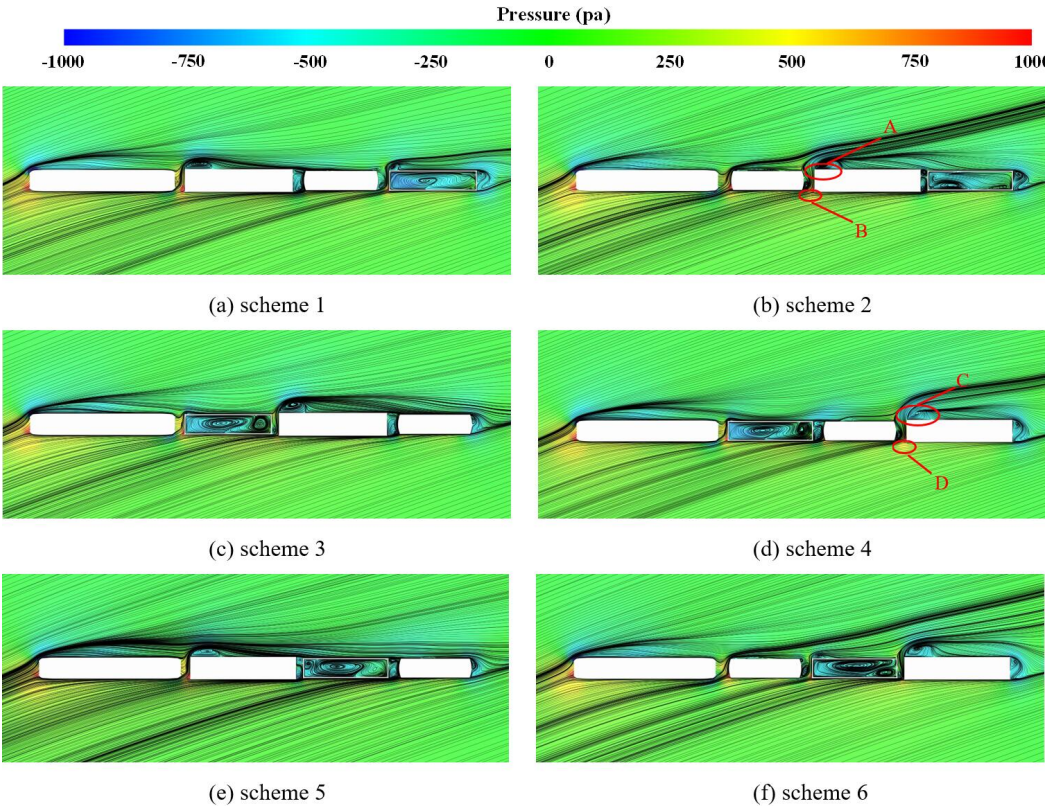

Fig. 13. The pressure distribution and streamline at the cut surface

corresponding negative pressure region (region A and region C) on the leeward side also increases. As shown in Figure 13 (b) and 13 (d), because the volume of the tank car is significantly smaller than that of the box car, it cannot effectively prevent the airflow from flowing to the boxcar, resulting in a large area of high pressure (region B and region D) on the windward side of the boxcar. The increase in the pressure difference between the windward and the leeward side is the direct cause of the increase in the lateral force of the box car.

Since the lateral force of the locomotive changes little, and the position of the boxcar will directly affect the changes of the lateral force of adjacent vehicles, the two cases when the lateral force of the boxcar is the largest and the smallest are selected (Scheme 2 and scheme 3) to compare and analyze. The positions of the three cross-sections are shown in Figure 14. The position of section A is based on the respective vortex center, and the positions of section B and section C are the same. The pressure distribution and the streamline of the cross section are shown in Figure 15.

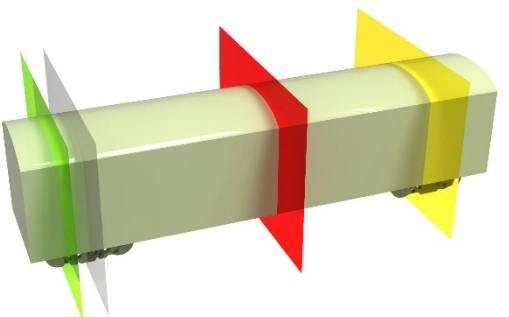

Fig. 14. Schematic diagram of the cross section of the box car

It can be seen from Figure 15 that when scheme 2 is adopted, at section A, the pressure on the windward side of the box car is higher than that on the windward side of the boxcar in scheme 3. The coverage of the negative pressure area on the leeward side of the box car is larger than that of scheme 3. In Section B and Section C, the pressure distribution on the windward side of the box car is similar, but the pressure in the center of the vortex on the leeward side of the box car near the underframe is smaller than that on the leeward side of the box car when scheme 3 is adopted. It can be seen from the pressure distribution of the three sections that when scheme 2 is adopted, the pressure difference between the windward side and leeward side of the boxcar is greater than that of scheme 3. It is the variation of pressure difference that causes the change of the lateral force of the boxcar, which is consistent with the previous analysis.

5. Conclusions

This paper simulated the aerodynamic performance of the freight train under crosswind. The influence of different marshalling forms on the aerodynamic performance of the freight train were compared and analyzed. Taking the three freight vehicles selected in this study as an example, in a crosswind environment, the best marshalling form is: locomotive--gondola car--box car--tank car. Both the aerodynamic drag of the train and the lateral force of the boxcar are the smallest by taking this marshalling form. In the actual marshalling process, there are many different types and quantities of freight cars.

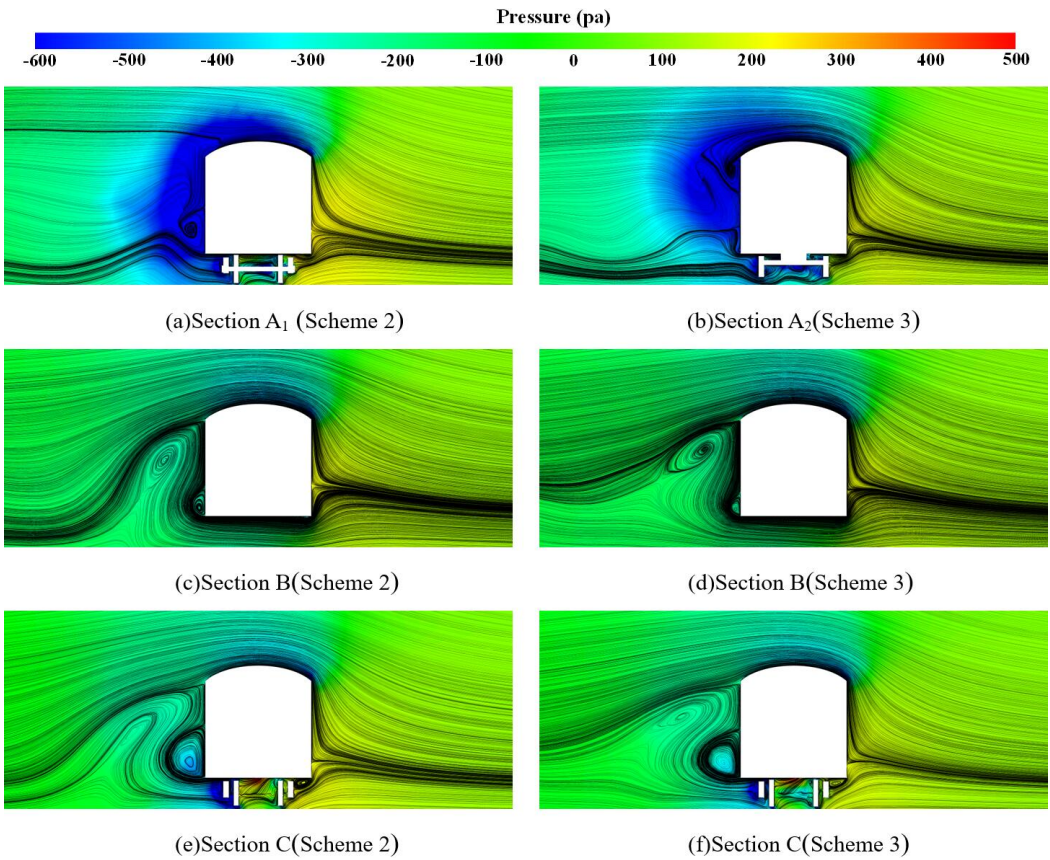

Fig. 15. Streamline and pressure distribution at different sections of the box car

The aerodynamic performance of each vehicle should be fully considered, and a reasonable marshalling form should be adopted to improve the aerodynamic performance of freight trains. The following conclusions are drawn:

1) The marshalling form has a significant influence on the aerodynamic performance of freight trains, and the difference of aerodynamic drag between different marshalling forms can reach a maximum of 20.8%. The marshalling form has little influence on the lateral force of the whole train, but has a greater influence on the change of the lateral force of a single vehicle, and the maximum difference can reach 24.1%.
2) Among the mixed freight trains, the box car is the largest one except the locomotive, which has the greatest impact on the aerodynamic performance of the train. The vehicle behind the box car can significantly reduce the aerodynamic drag, and the vehicle with a volume similar to the box car can also significantly reduce the drag when it is in front of the box car. Since the rear of the train has a large negative pressure region, it is necessary to avoid placing the vehicles with large volume such as box cars at the end to reduce the lateral force and the air resistance of the freight cars with large volume.
3) Due to its special cavity structure, the unloaded gondola car can significantly reduce the resistance of the following vehicles, especially when the empty gondola car is placed in front of the vehicles with large volume such as the box car. So the resistance of the vehicle with large volume can be reduced by the gondola car. The pressure in the rear area of the gondola car can be increased through the obstructive effect of large volume vehicles on the airflow, thereby reducing the differential pressure drag of the gondola, and the air resistance of the gondola car could be reduced. When the gondola car is in front of the box car, because the shapes of the side wall and the end wall of the gondola car is close to that of the box car, the distance between the two cars is close. The obstruction of the airflow brought by the gondola car can effectively reduce the pressure near the windward side of the front end wall of the boxcar, making the lateral force of the box car decrease. In the actual marshalling process, the unloaded gondola car should be placed in front of the large vehicles to effectively improve the aerodynamic performance of the train.
4) Due to its small volume and streamlined structure, the tank car has a small proportion in the total air resistance of the freight train compared with other freight vehicles. However, this kind of small freight cars should be placed behind the large freight cars such as box cars, which can not only reduce the resistance of the small vehicles themselves, but also avoid the situation that the resistance of the large vehicles behind them will increase due to their small volume and little blocking effect on the airflow. Since the front and rear ends of the tank are not flat, the distance between the tank and the end wall of the truck behind it varies. The change of distance will increase the vortex volume and the negative pressure area on the leeward side of the vehicle with large volume behind it, which will lead to the increase of lateral force of the vehicle. Therefore, in the actual marshalling process, placing the tank car behind the large vehicle can effectively avoid its negative impact on the aerodynamic performance of the train.

Acknowledgments

This study was funded by National Natural Science Foundation of China (Grant No. 11732014,11962013).

References

[1] Baker, C. (2010). The flow around high speed trains. *Journal of Wind Engineering & Industrial Aerodynamics,* 98, 277–298.
[2] Chen Z., Liu T., Jiang Z., et al. (2018). Comparative analysis of the effect of different nose lengths on train aerodynamic performance under crosswind. *Journal of Wind Engineering & Industrial Aerodynamics,* 78, 69-85.
[3] Cheli F., Ripamonti F., Rocchi D., et al. (2010). Aerodynamic behaviour investigation of the new EMUV250 train to cross wind. *Journal of Wind Engineering & Industrial Aerodynamics,* 98, 189–201.
[4] Flynn D., Hemida H., Soper D., et al. (2014). Detached-eddy simulation of the slipstream of an operational freight train. *Journal of Wind Engineering & Industrial Aerodynamics,* 132, 1-12.

[5] Flynn D., Hemida H., Baker C., (2016). On the effect of crosswinds on the slipstream of a freight train and associated effects. *Journal of Wind Engineering & Industrial Aerodynamics,* 156, 14-28.

[6] Gao G., Tian H., Yao S., et al. (2004). Effect of strong cross-wind on the stability of trains running on the Lanzhou-Xinjiang railway line. *Journal of China Railway Society,* 26(4), 36-40[in Chinese].

[7] Huo S., Liu T., Yu M., et al. (2020). Impact of the trailing edge shape of a downstream dummy vehicle on train aerodynamics subjected to crosswind. *Proceedings of the Institution of Mechanical Engineers, Part F: Journal of Rail and Rapid Transit,* 0(0), 1–14.

[8] Hemida H., Krajnović S., (2010). LES study of the influence of the nose shape and yaw angles on flow structures around trains. *Journal of Wind Engineering & Industrial Aerodynamics,* 98, 34-46.

[9] Krajnović S., Ringqvist P., Nakade K., et al. (2012). Large eddy simulation of the flow around a simplified train moving through a crosswind flow. *Journal of Wind Engineering & Industrial Aerodynamics,* 110, 86-99.

[10] Liu D., Wang T., Liang X., et al. (2020). High-speed train overturning safety under varying wind speed conditions. *Journal of Wind Engineering & Industrial Aerodynamics,* 198, 104111.

[11] Mao J, Ma X., Xi Y., (2011). Research on the running stability of high-speed trains under the cross wind by means of simulation. *Journal of Beijing Jiaotong University,* 35(1), 44-48+53[in Chinese].

[12] Niu J., Zhou D., Wang Y., (2018). Numerical comparison of aerodynamic performance of stationary and moving trains with or without windbreak wall under crosswind. *Journal of Wind Engineering & Industrial Aerodynamics,* 182, 1-15.

[13] Niu J., Zhou D., Liu T., et al. (2017). Numerical simulation of aerodynamic performance of a couple multiple units high-speed train. *Vehicle System Dynamics,* 55(5), 681-703.

[14] Östh J., Krajnović S., (2014). A study of the aerodynamics of a generic container freight wagon using Large-Eddy Simulation. *Journal of Wind Engineering & Industrial Aerodynamics,* 44, 31-51.

[15] Sterling M., Baker C., Jordan S., et al. (2008). A study of the slipstreams of high-speed passenger trains and freight trains. *Proceedings of the Institution of Mechanical Engineers, Part F: Journal of Rail and Rapid Transit,* 222, 177-193.

[16] Sima M., Eichinger S., Blanco A., et al. (2015). Computational fluid dynamics simulation of rail vehicles in crosswind: Application in norms and standards. *Proceedings of the Institution of Mechanical Engineers, Part F: Journal of Rail and Rapid Transit,* 229(6), 635-643.

[17] Wu, Z., Yang, E., Ding, W., (2017). Design of large-scale streamlined head cars of high-speed trains and aerodynamic drag calculation. *Archives of Transport*, 44(4), 89-97.

[18] Wu, Z., Huo, Y., Ding, W., et al., (2018). Bionic shape design of electric locomotive and aerodynamic drag reduction. *Archives of Transport*, 48(4), 99-109.

[19] Wang Z., Li T., Zhang J., (2018). Research on aerodynamic performance of high-speed train subjected to different types of crosswind. *Journal of Mechanical Engineering,* 54(4), 203-211[in Chinese].

[20] Xi Y., Mao J., Gao L., et al. (2015). Aerodynamic force/moment for high-speed train in crosswind field based on DES. *Journal of Central South University,* 46(3), 1129-1139[in Chinese].

[21] Xiong X., Liang X., Jin Q., (2015). Numerical simulation of aerodynamic force on tarpaulin of railway vehicle under cross wind condition. *Journal of Central South University,* 46(2), 728-735[in Chinese].

[22] Yang Z., Ma J., Chen Y., et al. (2010). The Unsteady Aerodynamic Characteristics of a High-speed Train in Different Operating Conditions under Cross Wind. *Journal of China Railway Society,* 32(2), 18-23[in Chinese].

[23] Zhou D., Tian H., Yang M., et al. (2007). Comparison of aerodynamic performance of different kinds of wagons running on embankment of the Qinghai Tibet railway under strong cross wind. *Journal of China Railway Society,* 29(5), 32-36[in Chinese].